International Communications in Heat and Mass Transfer 158 (2024) 107885

Contents lists available at ScienceDirect

International Communications in Heat and Mass Transfer

journal homepage: www.elsevier.com/locate/ichmt

# Optimizing thermal efficiency: Advancements in flat plate heat exchanger performance through baffle integration

M. Nithya [a,*], M. Senthil Vel [b], S. Anitha [c], C. Sivaraj [a]

[a] Department of Mathematics, PSG College of Arts and Science, Coimbatore 641014, Tamil Nadu, India
[b] Department of Mechanical Engineering, PSG Institute of Technology and Applied Research, Coimbatore 641062, Tamil Nadu, India
[c] Department of Mathematics, PSG Institute of Technology and Applied Research, Coimbatore 641062, Tamil Nadu, India

ARTICLE INFO

*Keywords:*
Plate heat exchanger
Computational fluid dynamics
Baffle
Power plant
Thermal performance

ABSTRACT

Compact heat exchangers have been gaining popularity in many industrial applications. Various types of passive turbulising structures such as corrugations, protrusions and ribs are introduced in the flow path to increase the effective heat transfer area and the level of turbulence in the flow path. This study investigates the impact of introduction of baffles on the performance of PHEs in terms of flow characteristics, pressure drop, and heat transfer. Two distinct types of baffle structures, namely wedge and aerofoil configurations, were introduced at varying numbers - 1, 3, and 5. An extensive experimentation is conducted for a FPHE in a thermal power plant of 500 × 2 MW and various flow and thermal parameters are measured. Computational Fluid Dynamics is utilized in this study to find the optimum baffle configuration. A detailed validation study is executed to obtain the correct computational algorithm, that is the right mesh count, optimum turbulence model, and precise numerical algorithm by comparing the numerical results with the available experimental results. Wedge- type baffles create increased turbulence and pressure drop, while aerofoil-type baffles minimize stagnation and exhibit lower pressure drop. Both baffle configurations lead to a substantial increase in heat transfer, with the 5-wedge-baffle setup showing the highest up to a 55% enhancement of Nusselt number. The Performance Evaluation Criterion (PEC) of wedge and aerofoil type is about 1.24 to 1.3 and 1.22 to 1.24 to that of conventional one respectively.

## 1. Introduction

PHEs are eminently being used in industries such as thermal power plants, nuclear plants, and pharmaceutical industries because of their compact size and low weight, superior thermal performance, and ease of cleaning. The PHE was first debuted in Germany in the 1870s [1]. The gasketed PHEs market was estimated at 3.1 billion globally in 2021 and is anticipated to grow to 5.1 billion by 2031. Due to COVID-19's peak, gasketed PHE system manufacturing was halted, which declined sales but performed well after their manufacture resumed due to increased GPHE use in medical, oil, gas, and food industries worldwide, the market will rise significantly in the next years [2]. Moreover, different experimental studies and industry testing reveal that PHE fouling is 5 to 20 times lower than shell and tube heat exchangers for the same workload and process circumstances in heating water solutions [3].

The broad requirements for research in heat exchangers include: How to design more compact heat exchangers, have higher thermal efficiency, achieve a balance between increased heat transfer and the resulting pressure drop, manufacturing techniques, fouling, and material problems, primarily in applications involving high temperatures and erratic operation. Different types of enhancement strategies, such as passive, active, and hybrid procedures, have been used [4].

In the pursuit of enhancing convective heat transfer efficiency, Amnart and Jedsadaratanachai [5] introduced double-V baffles to create a vortex and impinging flows, thereby disrupting the thermal boundary layer on the circular tube's isothermal surface. Meanwhile, Soliman et al. [6] conducted a numerical analysis involving different rib types within an FPHE. Their results highlighted that the rectangular ribs outperformed the others, exhibiting the highest thermal-hydraulic parameters, with values of 1.62 for the hot side and 1.84 for the cold air side.

Montazerifar et al. [7] for the first time designed novel fractal fins and analyzed oil/MWCNT turbulent flow at six angles of attack on the multi-stream plate-fin heat exchanger performance. The results showed that maximal flow impingement occurs at higher *Re* and that fluid mixing improves at maximum fractal fin angles of attack. Researchers studied the different types of inserts, that function as a vortex generator,

* Corresponding author.
*E-mail addresses:* msdnithya@gmail.com (M. Nithya), msv@psgitech.ac.in (M. Senthil Vel), anitha@psgitech.ac.in (S. Anitha), vcsivaraj@gmail.com (C. Sivaraj).

https://doi.org/10.1016/j.icheatmasstransfer.2024.107885

Available online 3 August 2024

**Nomenclature**

| | |
|---|---|
| A | Heat transfer area, $m^2$ |
| $c_p$ | Specific heat capacity, J/(kgK) |
| $d_h$ | Hydraulic diameter, m |
| D | Port diameter, m |
| $f$ | Skin friction factor |
| $f_r$ | Relative friction factor |
| h | Convective heat transfer, $W/(m^2K)$ |
| k | Thermal conductivity, W/(mK) |
| $\dot{m}$ | Mass flow rate, kg/s |
| MW | Mega watt |
| Nu | Nusselt number |
| PEC | Performance Evaluation Criterion |
| Q | Heat transfer rate, W |
| St | Stanton Number |
| $St_r$ | Relative Stanton number |
| T | Temperature of the fluid, K |
| $\Delta T$ | Temperature difference, K |
| $T_b$ | Bulk mean temperature, K |
| $T_{cell}$ | Temperature of a cell in the computational domain, K |
| $T_{ref}$ | Reference temperature, K |
| $T_{wall}$ | Wall temperature, K |
| TKE | Turbulent Kinetic Energy |
| $u_T$ | Shear velocity, m/s |
| $V_{avg,h}$ | Average velocity in the hot side, m/s |
| $V_x$ | Velocity in the direction of x, m/s |
| $V_y$ | Velocity in the direction of y, m/s |
| $V_z$ | Velocity in the direction of z, m/s |

*Greek symbols*

| | |
|---|---|
| $\kappa$ | Turbulent Kinetic Energy, $m^2/s^2$ |
| $\rho$ | Density, $kg/m^3$ |
| $\mu$ | Viscosity, $(Ns)/m^2$ |
| $\mu_t$ | Eddy viscosity, $(Ns)/m^2$ |
| $\tau_w$ | Wall shear stress, $N/m^2$ |

*Subscripts*

| | |
|---|---|
| b | Baffled FPHE |
| c | Conventional FPHE |
| r | Relative factor |

by varying their sizes and shapes. These investigations demonstrate that heat transfer and pressure drop are increased while exergy losses are reduced by putting inserts into PHE channels [8–12]. N. K. Pandya et al. [13] also modified the Wilson Plot method for finding heat transfer coefficients.

Gherasim et al. [14] analyzed water flow in a CPHE, assessing Nusselt number, friction factor, and temperature distribution under laminar and turbulent conditions. Temperature measurements from the plate's exterior surface indicated the most significant gradient occurred at the side plate, with the highest and lowest temperatures at the hot and cold inlets, respectively. The undulations in the Pillow plate heat exchanger (PPHE) channels improve heat transfer by enhancing fluid boundary layer aeration, but further optimization is needed for PPHE to compete with CPHE. CFD simulations were done to examine the impact of the dimples. Piper et al. [15] modified the conventionally undulating surface with the addition of supplementary dimple features. Hence, fluids are better-mixed close to the wall because the dimples frequently disrupt the turbulent boundary layer. When compared to conventional PPHE, the novel channel improves thermo-hydraulic efficiency by 11.2%. And also, more importantly, this novelty enhances heat transfer and also reduces the pressure drop.

Fuji et al. [16] were the pioneers in examining the impact of various types of surface roughness on natural convection. Kang et al. [17] observed that equilateral triangular ducts with increased surface roughness exhibited improved heat transfer efficiency in their experimental studies, albeit at the expense of higher friction losses. Research focusing on the influence of surface roughness on PHEs has revealed a direct correlation between increased roughness and enhanced heat transfer, accompanied by a notable rise in pressure drop [18–21].

In experimental investigations using R12 as the working fluid, the study of pressure drop and evaporative heat transfer in vertical smooth and cross-ribbed flat channels was conducted [22]. Cross-ribbed channels displayed three times the heat transfer coefficient compared to their smooth counterparts. In both types of channels, up-flow exhibited 30–70% higher heat transfer coefficients than downflow.

Giovanni et al. [23] conducted an experimental study on a vertically positioned, transversely truncated square-ribbed plate. They examined the impact of rib size, pitch, and the number of truncations. Vertical smooth surfaces showed increased heat transfer primarily due to the arrangement of truncated ribs.

In a recent numerical analysis by [24], the effect of zigzag ribs was investigated, resulting in an increase of over 4% in the average heat transfer coefficient and an 11% rise in heat transfer area compared to a flat surface.

Nghana et al. [25] employed statistical modelling to study turbulent natural convection in vertical and inclined channel s featuring repeating triangular, square, circular, and semicircular ribs. Their findings demonstrated substantial heat transfer improvements compared to smooth channels, with triangular ribs performing the best. Furthermore, due to increased turbulence, broken ribs outperformed continuous ribs.

In an experiment conducted by Nilpueng and Wongwises [26], three symmetric chevron plates were used, with surface roughness created through sandblasting. The results of this experiment demonstrated that, compared to a smooth surface, increased surface roughness led to a 4.46–17.95% rise in heat transfer coefficient and a 3.90–19.24% increase in pressure drop.

Gulenoglu et al. [27] also experimented to assess the performance of three chevron plates with distinct geometric characteristics. Their findings underscored the profound impact of geometrical parameters, including enlargement factor, port diameter, and channel flow area, on the thermal and hydraulic performance of heat exchangers.

Al-zahrani et al. [28–30] introduced a modified PHE featuring a novel gasket design. This PHE exhibited a remarkable increase in *Nu* and f data, reaching up to 70% and 4.4 times that of the basic PHE, respectively. Al-zahrani et al. [31] further implemented another passive technique, transforming the PHE to incorporate two mid-gaskets and the overall thermal performance is evaluated by determining the ratio of the heat transfer rate to the increase in pumping power, known as the JF factor. The JF data for the PHE with two mid-gaskets surpassed those of the PHE with one mid-gasket and the conventional PHE. Furthermore, this modified PHE displayed superior velocity compared to the conventional one.

Baffles are commonly employed in various heat exchanger designs to induce turbulence, promote better mixing of fluids, and enhance heat transfer rates. They effectively disrupt the flow of fluids within the exchanger, encouraging better thermal performance and more efficient heat transfer. While traditional heat exchangers like shell and tube configurations [32–37] often incorporate baffles to enhance thermal and hydrodynamic characteristics, there is a notable gap in the existing literature regarding the application of baffles in PHEs and their subsequent impact on heat transfer performance. The focus of this discussion is to shed light on the potential benefits and implications of

incorporating baffles in PHEs, with an emphasis on enhancing heat transfer efficiency along with minimizing the increase in pressure drop. In this study, baffle was introduced for the first time in the FPHE to create turbulence in the fluid flow. Initially a wedge-configured baffle was investigated for various number of baffles and further the investigation was carried out for an aerofoil-configuration for the purpose of reducing the pressure drop. A comparative analysis between these configurations and the conventional one (no baffle) is conducted to determine the optimal configuration.

## 2. Experimental approach

### 2.1. Need for experimentation

The numerical analysis involves a multitude of factors, including the number of variables, mesh parameters such as count, shape, and node spacing, as well as considerations for capturing fine details through appropriate mesh selection. Other crucial aspects encompass the choice of a turbulence model, pressure-velocity coupling method, discretization method, order of discretization, and the criteria for convergence. To ensure the reliability of the numerical results, an exclusive experimental investigation is imperative.

### 2.2. Experimentation procedure for validation study

In this study, validation of the numerical results calculated by the CFD procedure is compared with the results of the experimentation conducted at the Joint Venture Power Plant of Tamil Nadu and Central of 500 × 2 MW. The objective of this experiment is to evaluate the precision and reliability of the numerical model utilized in this study.

The flow of DM water (hot fluid) and seawater (coolant) is controlled by a regulator valve, with both fluids pumped in counter direction. Temperature transducers near the inlet and outlet ports measure the temperatures of the working fluids, while pressure is monitored by a Gauge Pressure Transmitters near the outlet ports.

The flowchart given in Fig. 1. represents the cooling process of DM water by seawater. The experimental setup of the respective PHE is shown in Fig. 2.

### 2.3. Error analysis and uncertainty prediction

The manufacturer conducted an instrumentation calibration to rectify systematic errors, and to minimize random errors, multiple readings were taken for each experiment and subsequently averaged. Additionally, a thorough uncertainty analysis was performed in Table 1, evaluating the impact of uncertainties (UR) using the expression proposed by Kline and McClintock [38].

## 3. Methodology

### 3.1. Model description

The gasketed FPHE employed in this context features a plate with a length of 2508 mm and a thickness of 0.6 mm as shown in Fig. 3. (a). The heat exchanger operates in a counterflow direction, and the working fluids utilized are demineralized (DM) water and seawater. Also, the dimensions specified for the plate align with those utilized in experimental validation here. Given the substantial size of this industrial plate, three plates are utilized for this study.

The baffle, considered here is of a series of triangles (sharp edges) with space in between for the fluid flow. This baffle is located at the end of the distribution area so that fluid tends to spread evenly and create turbulence motion in the initial flow of fluid itself. Based on the study of the latter, the newly designed baffle is modified again to give better performance through reducing pressure drop. This newly improved baffle has captured the design of aerofoil (smooth edges). Fig. 3. (b-d) represents the arrangements of the baffles along the plates. The geometry and dimensional details of wedge and aerofoil baffles are as seen in Fig. 3. (e-h). In this study, the number of baffles is varied and the resulting Nu, St, skin friction factor, PEC, relative *f*, and relative St were studied numerically using a new CFD approach for the Re range of 100 to 2000.

### 3.2. Need for an innovative meshing approach

As the overall computational domain is of very small thickness general tetrahedron approach of domain discretization would result in a

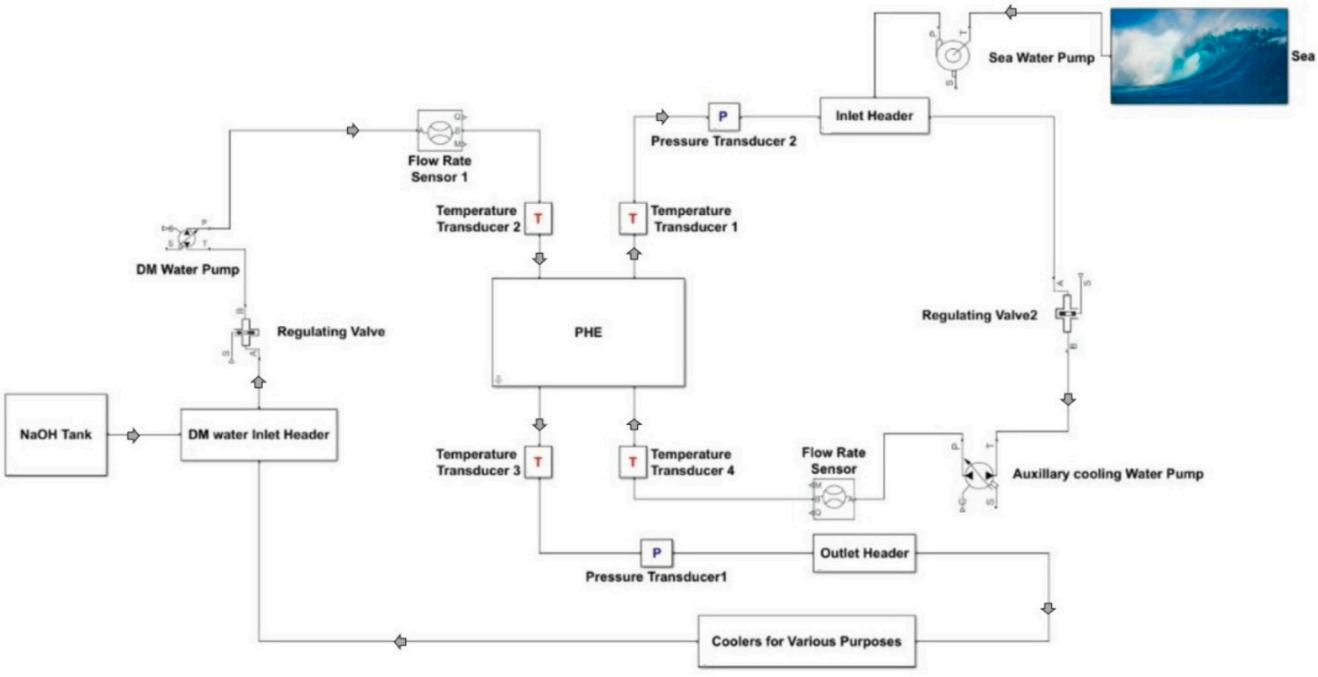


**Fig. 1.** Flow chart of the experimental setup in the Thermal Power Plant.

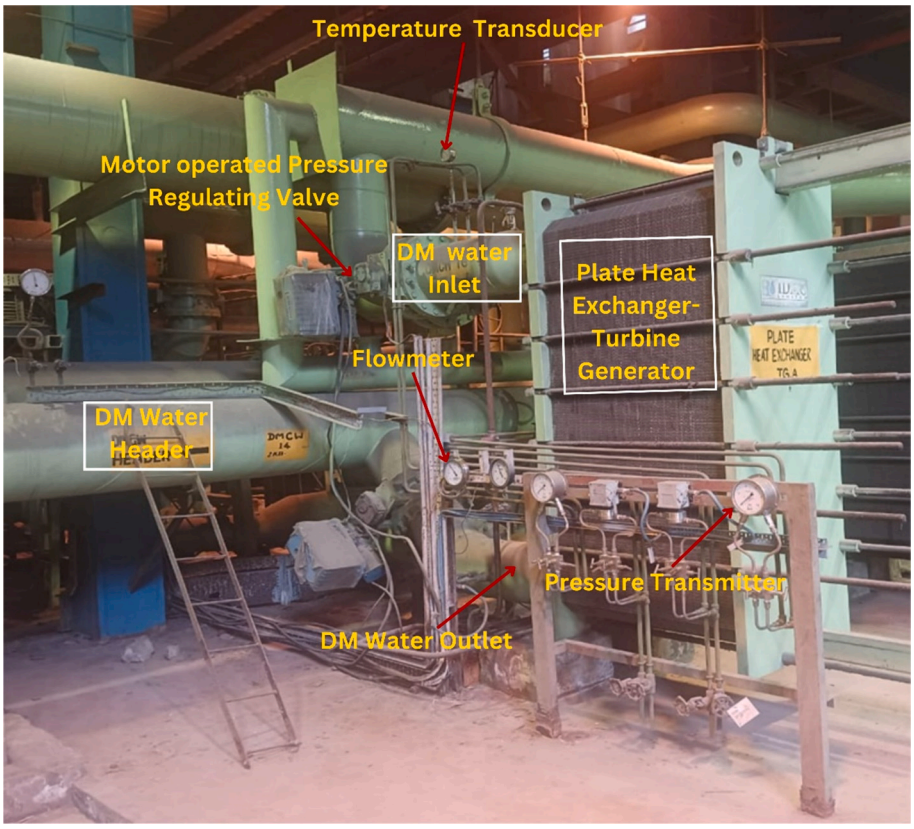


**Fig. 2.** Image of the experimental setup.

**Table 1**
The uncertainty values for variables.

| Variable | Uncertainty |
|---|---|
| Hot water inlet Temperature | ± 0.15 °C |
| Cold water inlet Temperature | ± 0.15 °C |
| Hot water outlet Temperature | ± 0.15 °C |
| Cold water outlet Temperature | ± 0.15 °C |
| Mass flow rate of hot side | ± 3% |
| Mass flow rate of cold side | ± 3% |
| Channel equivalent diameter | ± 2% |
| Heat transfer rate of hot side | ±6% |

very high mesh count. This would in turn increase the total computational time and effort significantly. To overcome such difficulty a novel meshing approach is used from the planar surface mesh using a sweep algorithm depicted in Fig. 4. (a & b). The sweep meshing technique generates a high-quality mesh using fewer nodes compared to alternatives like the free mesher [39]. Structured Hexahedron volume elements are created in ANSYS Mesher shown in Fig. 4. (c). The surface grids over wedge and aerofoil baffles are seen in Fig. 4. (d & e). Conformal interfacing of all mesh nodes is assured in the entire computational domain. This methodology reduces the mesh count considerably at least one-third from unstructured tetrahedron at the same time aids in increasing the accuracy of the solution. The increase in solution accuracy is attributed to the reason that all elements are faced parallel to each other and are aligned perpendicular to the flow direction. A comprehensive grid independence study is performed to find the optimum mesh count.

### 3.3. Transport equations for fluid flow with heat transfer

Eqns. (1–5), which serve as the governing equations, were resolved using the commercially available Ansys Fluent 2018 software. Subsequently, various additional parameters were computed as well. Transport equations for turbulence properties are mentioned separately is given in the Eqns. (20 and 21).

Continuity equation:

$$\frac{\partial(\rho V_x)}{\partial x}+\frac{\partial(\rho V_y)}{\partial y}+\frac{\partial(\rho V_z)}{\partial z}=0 \tag{1}$$

- Momentum equation in x direction:

$$\rho\left(\frac{\partial V_x}{\partial t}+V_x\frac{\partial V_x}{\partial x}+V_y\frac{\partial V_x}{\partial y}+V_z\frac{\partial V_x}{\partial z}\right)=-\frac{\partial P}{\partial x}+(\mu+\mu_t)\left(\frac{\partial^2 V_x}{\partial x^2}+\frac{\partial^2 V_x}{\partial y^2}+\frac{\partial^2 V_x}{\partial z^2}\right) \tag{2}$$

- Momentum equation in y direction:

$$\rho\left(\frac{\partial V_y}{\partial t}+V_x\frac{\partial V_y}{\partial x}+V_y\frac{\partial V_y}{\partial y}+V_z\frac{\partial V_y}{\partial z}\right)=-\frac{\partial P}{\partial y}+(\mu+\mu_t)\left(\frac{\partial^2 V_y}{\partial x^2}+\frac{\partial^2 V_y}{\partial y^2}+\frac{\partial^2 V_y}{\partial z^2}\right) \tag{3}$$

- Momentum equation in z direction:

$$\rho\left(\frac{\partial V_z}{\partial t}+V_x\frac{\partial V_z}{\partial x}+V_y\frac{\partial V_z}{\partial y}+V_z\frac{\partial V_z}{\partial z}\right)=-\frac{\partial P}{\partial z}+(\mu+\mu_t)\left(\frac{\partial^2 V_z}{\partial x^2}+\frac{\partial^2 V_z}{\partial y^2}+\frac{\partial^2 V_z}{\partial z^2}\right) \tag{4}$$

- Conservation of energy:

$$\rho C_p\left(V_x\frac{\partial T}{\partial x}+V_y\frac{\partial T}{\partial y}+V_z\frac{\partial T}{\partial z}\right)=k\nabla^2 T \tag{5}$$

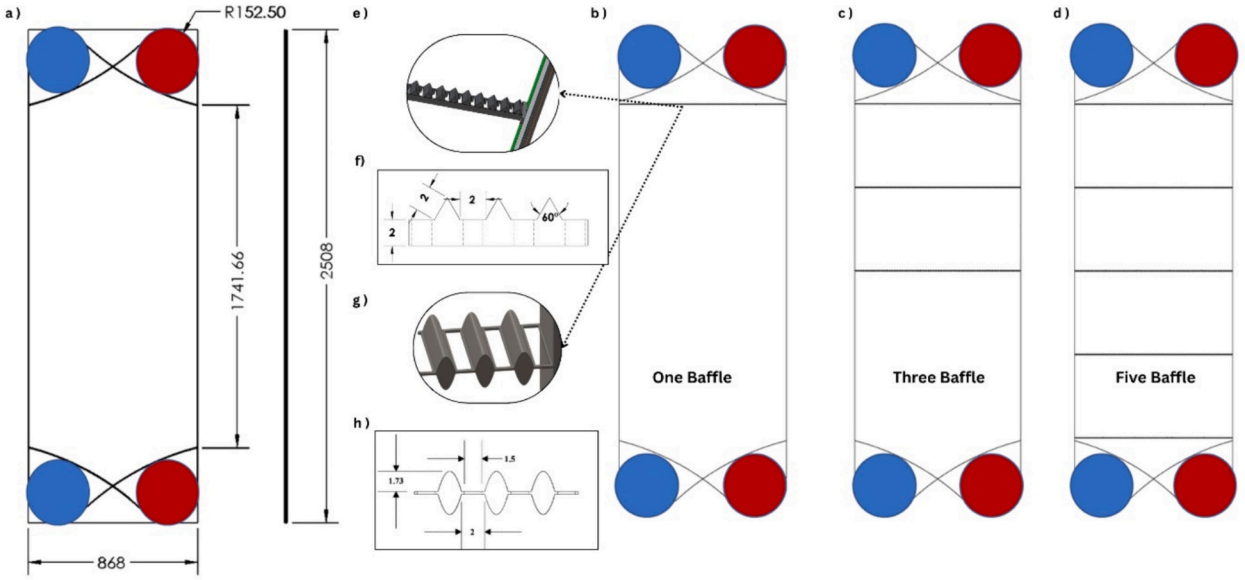


**Fig. 3.** (a) Geometry of conventional FPHE (b - d) Baffle configurations of modified (e & f) Geometry of wedge baffle (g & h) Geometry of aerofoil baffle.

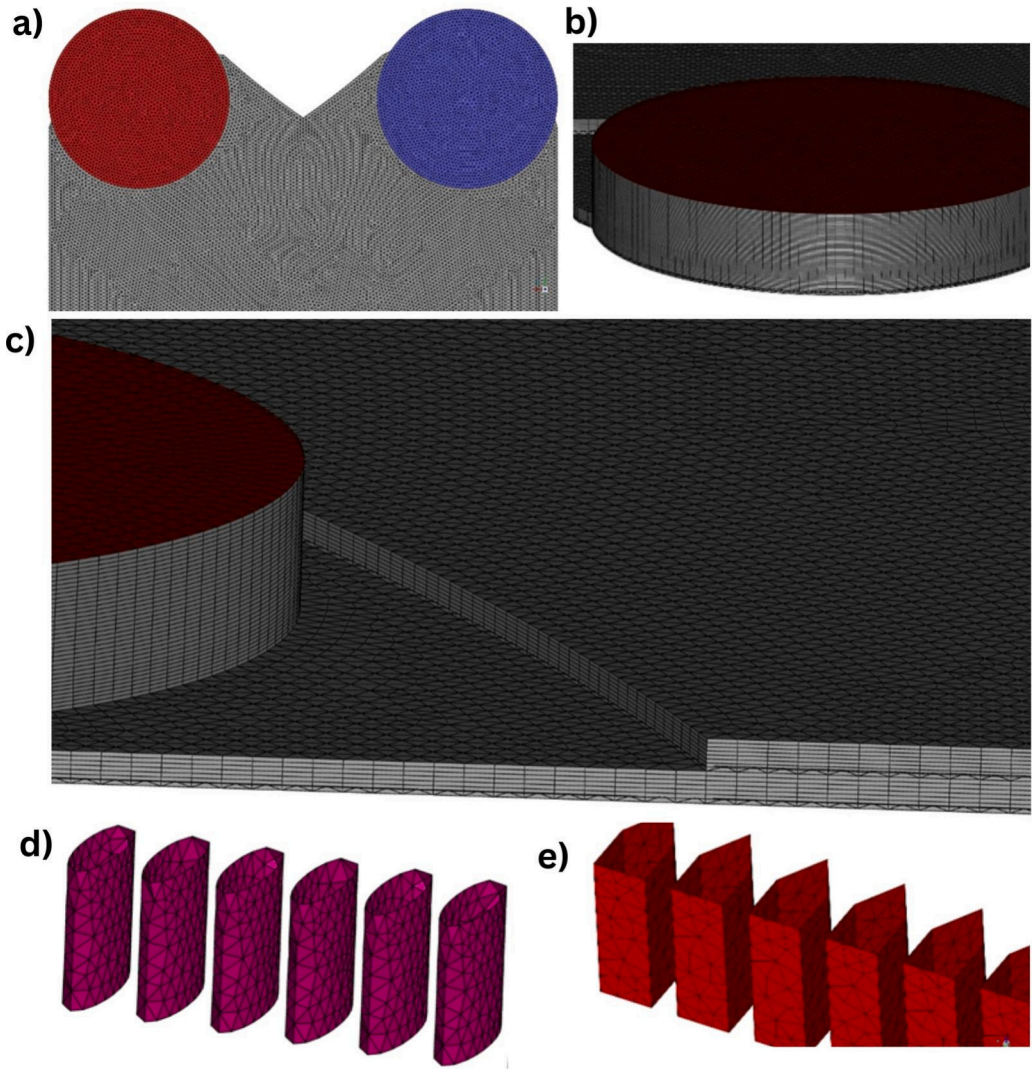


**Fig. 4.** (a) Tri surface elements (b) Hex elements generated using Sweep algorithm (c) A cut section of the volume mesh (d) Wedge baffles with surface grid (e) Aerofoil baffles.

### 3.4. Data formulation

The convective heat transfer coefficient and the rate of heat transfer is given in Eqns. (6&8).

$$h = \frac{\rho c_p {c_\mu}^{1/4} \kappa^{1/2}}{T^+} \tag{6}$$

where $c_\mu (= 0.09)$ is the proportionality constant and $T^+$ is the non-dimensional temperature as defined in Eq. (7).

$$T^+ = f(y^+) \tag{7}$$

where $y^+$is the non-dimensional distance of the first cell centroid from the wall. The relation between $T^+$and $y^+$depends on the type of wall function used.

$$Q = \frac{(T_{wall} - T_{cell}) \rho c_p {c_\mu}^{1/4} k^{1/2}}{T^+} A \tag{8}$$

The mass average temperature for an internal flow is defined as.

$$T_{cell} = T_{ref} = \frac{\int T\rho \left|\vec{V}.d\vec{A}\right|}{\int \rho \left|\vec{V}.d\vec{A}\right|} = \frac{\sum_{i=1}^{n} T_i \rho_i \left|\vec{V_i}.\vec{A_i}\right|}{\sum_{i=1}^{n} \rho_i \left|\vec{V_i}.\vec{A_i}\right|} \tag{9}$$

Essential parameters such as Nusselt number Eq. (10), Stanton number Eq. (11) Reynolds number Eq. (12) are:

$$Nu = \frac{h\, d_h}{k} \tag{10}$$

$$St = \frac{h}{\rho V c_p} \tag{11}$$

$$Re = \frac{\rho V_{avg,h}\, d_h}{\mu} \tag{12}$$

where,

$$d_h = \frac{4 * Port\ Area}{Port\ Wetted\ Perimeter} = \frac{4 * \left(\frac{\pi D^2}{4}\right)}{\pi D} = D \tag{13}$$

The skin friction factor Eq. (14) is described as,

$$f = \frac{2\tau_w}{\rho V^2} \tag{14}$$

The relative friction factor and Stanton number are given by Eqns. (15 & 16),

$$f_r = \frac{f_b}{f_c} \tag{15}$$

$$St_r = \frac{St_b}{St_c} \tag{16}$$

The thermal enhancement factor, also known as the Performance Evaluation Criterion (PEC), compares a modified PHE to the traditional one as given by Eq. (17),

$$PEC = \frac{St_b/St_c}{(f_b/f_c)^{1/3}} = \frac{St_r}{(f_r)^{1/3}} \tag{17}$$

### 3.5. Study of grid independence

Mesh independence is a crucial consideration in any CFD simulation. Achieving mesh independence is vital for obtaining accurate and reliable results, as an overly coarse mesh might lead to inaccurate approximations, while an excessively fine mesh can inflate computational costs without substantial improvements in precision.

In this study, the entire computational domain is discretized with an initial mesh of 3.6 million and varied with a constant factor of 1.2. Five trials were attempted with mesh count values of 4.32 million, 5.2 million, 6.2 million, 7.5 million, and 9 million. Numerical results become independent of the number of cells at 6.4 million. It is found that the convergence curve accords with such a mathematical formula:

$$y = f(x) = A + \frac{B}{x} + \frac{C}{x^2} + \frac{D}{x^3} + \ldots + \frac{Q}{x^n} = \sum_{i=0}^{n} \frac{a_i}{x_i} \tag{18}$$

where, $x$ represents the number of cells in the mesh, while $A$, $B$, $C$, and $Q$ are coefficients determined during the simulation. Each coefficient $a_i$ corresponds to a specific term in the equation, reflecting its contribution to the overall solution $y$.

As the mesh becomes finer, the solution progressively converges towards the true solution. It's important to note that the accuracy of the true solution depends on the mathematical methodologies employed and remains unaffected by changes in grid resolution. This concept is highlighted by Eq. (19), where 'a' symbolizes the grid-independent parameter in numerical simulations which demonstrates that as the number of cells tends towards infinity, the solution converges to a grid-independent parameter $a$.

$$\left(\frac{a}{x}\right)^i = 0\ i = 1, 2, \ldots, n\ so\ \lim_{i \to \infty} f(x) = a \tag{19}$$

The outcomes of the grid-independence study have been acquired and organized in the graph Fig. 5.

### 3.6. Study of appropriate turbulence model

Even though many contributions are available in the development of modelling methodology to numerically model turbulence [40], to date no turbulence model can be used unanimously for all types of turbulence flows. A wide range of turbulence models are being developed such as Eddy viscosity models (EVM), Reynolds stress model (RSM), Large eddy simulation (LES), etc., and are added to the commercial CFD packages [41]. Models such as RSM and LES are computationally very expensive thus EVM models are quite extensively utilized in industries.

Due to the complex nature of turbulent flows characterized by significant eddy differences on a large scale and considerable variability in the degree of turbulent intensity, the appropriate selection of turbulence models is mandatory.

This work utilises variants of k-ε model for one such important reason that it can use wall functions for the near wall modelling and eliminates the creation of an enormous mesh count. The geometrical intricacy and very small dimensional characteristics associated with bPHE is the key reason for utilising k-ε turbulence model. For the similar reason the k-ω turbulence model is not utilized in this study despite its advantage in modelling the near wall flow more accurately.

The realizable k-ε model featuring a scalable wall function has garnered favour among certain researchers [42–47] due to its demonstrated ability to produce highly accurate results closely matching experimental data. Additionally, it exhibits a commendable level of consistency across various Reynolds numbers.

CFD analysis are conducted for three different variants of k-ε models, namely, Standard, RNG and Realizable models and a careful selection of the most appropriate one is done.

The transport equations for k and ε in the realizable k-ε model are:

$$\frac{\partial}{\partial t}(\rho k) + \frac{\partial}{\partial x_j}(\rho k u_j) = \frac{\partial}{\partial x_j}\left[\left(\mu + \frac{\mu_t}{\sigma_k}\right)\frac{\partial k}{\partial x_j}\right] + G_k + G_b - \rho\varepsilon - Y_M + S_k \tag{20}$$

$$\frac{\partial}{\partial t}(\rho \varepsilon) + \frac{\partial}{\partial x_j}(\rho k u_j) = \frac{\partial}{\partial x_j}\left[\left(\mu + \frac{\mu_t}{\sigma_\varepsilon}\right)\frac{\partial \varepsilon}{\partial x_j}\right] + \rho C_1 S_\varepsilon - \rho C_2 \frac{\varepsilon^2}{k + \sqrt{\nu\varepsilon}} + C_{1\varepsilon}\frac{\varepsilon}{k} C_{3\varepsilon} G_b + S_\varepsilon \tag{21}$$

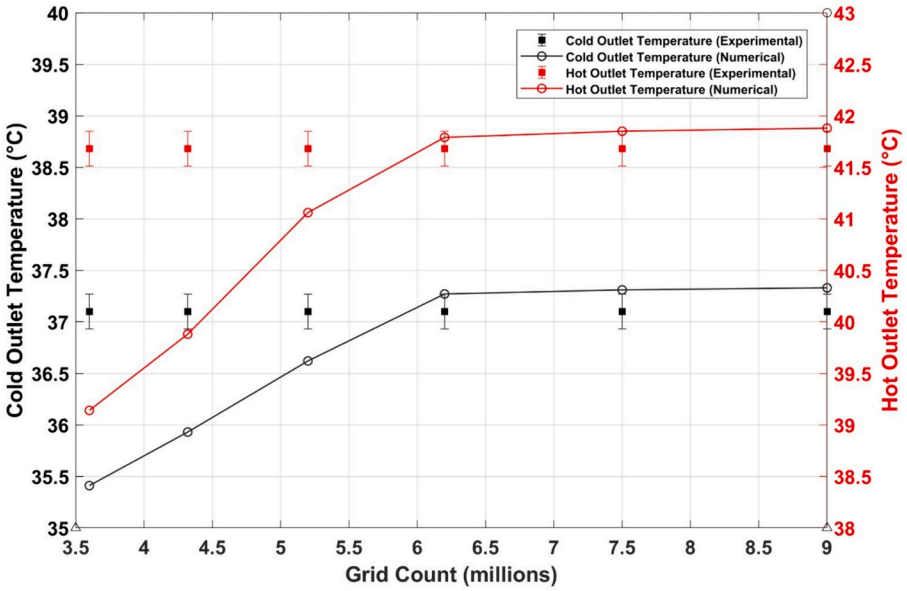


**Fig. 5.** Grid independence test for various outlet temperatures of both hot and cold sides.

where,

$$C_1 = max\left[0.43, \frac{\eta}{\eta+5}\right], \eta = S\frac{k}{\varepsilon}, S = \sqrt{2S_{ij}S_{ij}}$$

Here, $G_k$ and $G_b$ represents the generation of turbulent kinetic energy (TKE) caused, respectively, by mean velocity gradients and buoyancy, $Y_M$ represents the proportion of the total dissipation rate attributable to the fluctuating dilatation in compressible turbulence., $C_2$ and $C_{1\varepsilon}$ are constants, $\sigma_k$ and $\sigma_\varepsilon$ are the turbulent Prandtl numbers for k and ε, respectively. $S_k$ and $S_\varepsilon$ are user-defined source terms.

### 3.7. Selection of wall treatment method

Models for treating the near-wall region are crucial for precise simulation of turbulent flow, especially in the vicinity of the boundary layer [48]. Standard wall functions(SWF) apply the log law of the wall to describe the behavior of momentum and temperature, and they rely on y* [49]. The laws governing the mean velocity and temperature near the wall are grounded in the wall unit y*, rather than $y^+ = \rho u_T y/\mu$. Here, y represents the first cell height from the wall, $y^+$is the nondimensional form of the same and y* is the dimensionless distance from the wall. The Non-Equilibrium Wall Function (NEWF) has the potential to enhance outcomes in scenarios where near-wall flows face significant pressure gradients and exhibit strong non-equilibrium. Meanwhile, the Scalable Wall Function (SCWF) compels the incorporation of the log law alongside the standard wall function approach.

Following numerous experiments involving the three k-ε turbulence models alongside the three-wall function methodologies, a comparison was made between numerical results and experimental data. Notably, the realizable k-ε model with scalable wall functions consistently yielded the most accurate and reliable results, closely aligning with experimental findings across various *Re* which can be seen from the Fig. 6.

### 3.8. Solver conditions

- The flow is considered to be turbulent and steady, with three-dimensional characteristics.

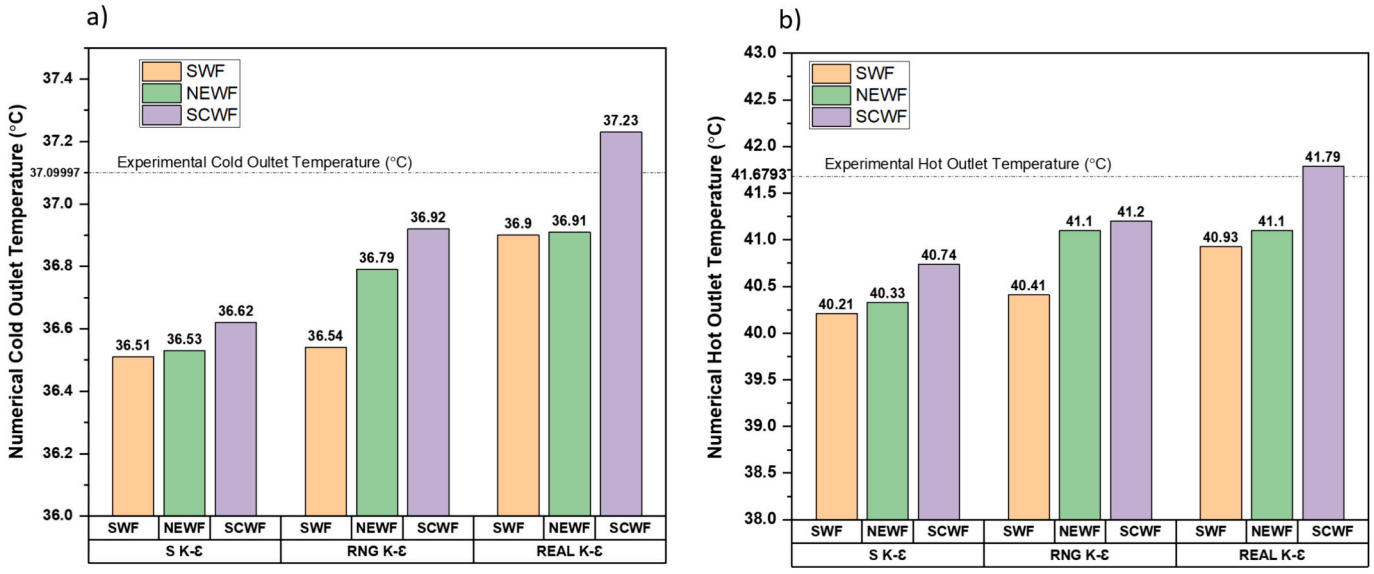


**Fig. 6.** Comparison study of numerical results with various turbulence models with industrial-experimental data a) Cold fluid b) Hot fluid.

- Fluid is assumed to be incompressible.
- Turbulence is modelled by the Eddy viscosity model (EVM) model and the appropriate turbulence model is selected from the outcome of the turbulence model study.
- The pressure-velocity coupling is achieved through the utilization of the PISO algorithm.
- A second-order approximation is employed for solving the flow, momentum, and turbulence equations.
- Water is assumed to be continuum fluid.

### 3.9. Physical properties of the fluid and boundary conditions

- Pressure inlet boundary condition is imposed at both inlet boundaries with a total pressure of 1 atm.
- Inlet temperature for hot fluid: 43°C
- Inlet temperature for cold fluid: 36°C
- Mass flow outlet boundary condition is imposed at both outlet boundaries with the following values.
- Mass flow rate for hot fluid: 2.76 kg/s
- Mass flow rate for cold fluid: 2.864 kg/s
- Walls are assumed to be adiabatic with no-slip conditions.

Further, the thermodynamic properties of both the fluids are given in Table 2.

### 3.10. Solver methodology

From the detailed validation study, the following conclusions are made:

- A mesh count of around 6.4 million is preferred for this study.
- Realizable k-ε model with scalable wall function.
- The PISO algorithm is used for pressure-velocity coupling.
- Second-order approximation is used for flow, momentum transport eqs.
- A first-order approximation is used in turbulent equations.
- The best practices in CFD, as determined through validation studies, are employed in subsequent CFD processes to examine the wedge-bPHE and aerofoil-bPHE under different configurations. In the case of the bPHEs, the velocity vector is evenly spread across, and there are only a few instances of recirculation observed in specific areas.

## 4. Results and discussion

The introduction of baffles significantly alters flow characteristics, including flow directionality, pressure drop, and flow residence time. To prevent stagnation on the front face of the baffles, they are designed to be either sharp-edged or smoothed, minimizing the frontal area. Velocity vector plots are illustrated in Fig. 7. (a & b) for conventional FPHE. In the case of wedge-type baffles, characterized by a bluff body, flow detachment occurs at the rear, leading to the formation of a visible wake zone as seen in Fig. 8. (a). This wake zone contributes to increased turbulence and pressure drop. Conversely, aerofoil-type baffles exhibit minimal stagnation at the front and a significantly smaller wake zone at the rear shown in Fig. 8. (b), resulting in a notably lower pressure drop compared to wedge-type baffles. To assess and compare the hydrodynamic and thermodynamic characteristics of seven different configurations under investigation, key parameters such as Nusselt number, Stanton number, and friction factor were considered.

**Table 2**
Properties and characteristics of fluid.

| Fluid | Density kg/m$^3$ | Viscosity kg/(ms) | Specific heat J/(kgK) | Thermal conductivity W/(mK) |
|---|---|---|---|---|
| DM water (hot) | 1000 | 0.0017 | 4190 | 0.56 |
| Sea water (cold) | 1025 | 0.001 | 3900 | 0.5 |

As the fluid flows through the space between them, the baffles cause a local acceleration of the fluid, leading to an enhanced fluid velocity. This acceleration results in an increased conductive heat transfer coefficient shown in Fig. 9. (a-d), ultimately boosting overall heat transfer.

Within the conventional FPHE turbulent intensity shown in Fig. 10. (a & c), a metric reflecting the mixing of hot and cold zones, is more pronounced at the inlets and outlets due to the 90-degree entry and exit of water into and out of the computational domain. In contrast, turbulent intensity is notably lower in other flow regions, indicating reduced heat transfer in the core region. However, Fig. 10. (b & d) show the significantly amplified turbulent intensity after the inclusion of baffles, leading to increased mixing of fluids in the region of hot and cold regions. In comparison to the wedge-type baffle configuration, aerofoil baffles exhibit lower turbulent intensity, so that the prior one provides enhanced fluid flow and mixing within the hot and cold zones.

The baffles also act as heat dissipation bodies by facilitating the conduction of heat from the hot fluid zone to the cold zone and vice versa. Subsequently, the fluid in each respective zone carries away this heat through convective processes, contributing to heightened heat transfer. The contour plot above illustrates thermal stratification along the baffle surface in both hot and cold regions. Furthermore, the thermal gradient along the baffle surface is slightly higher in wedge-type baffles when compared to aerofoil baffles.

The Nusselt number is computed for all configurations of PHEs and represented in the graph Fig. 11, revealing a substantial increase in heat transfer by up to 53% for the 5-wedge-baffle setup and up to 40% for the 5-aerofoil-baffle setup. Notably, the wedge baffles exhibit a more significant enhancement of about 10% in heat transfer compared to the aerofoil baffles. The higher TKE in the wedge-bPHE compared to the aerofoil-bPHE contributes to this enhancement, and it is directly proportional to the number of baffles and the Reynolds number.

Up to *Re* is 600, the graphs for all baffle cases tend to coincide, while noticeable distinctions emerge when *Re* surpasses 600. When *Re* attains the transition phase to a turbulent regime, wedge-bPHE with 3 and 5 baffles experiences a substantial increase, whereas 1-wedge and all aerofoil cases exhibit minimal change and nearly coincide. It is crucial to emphasize that all cases with baffles demonstrate a significant improvement compared to the conventional FPHE, highlighting the efficacy of baffle incorporation in enhancing performance.

The augmented heat transfer in the wedge-baffle configuration can be attributed to the geometry-induced alterations in fluid flow patterns and turbulence levels. The presence of wedge-shaped baffles creates vortices and promotes mixing, leading to enhanced convective heat transfer. To understand the behavior in various flow regimes namely laminar and turbulent *Re* is varied from 100 to 2000.

The higher TKE in the wedge-bPHE suggests a more energetic and turbulent flow within the heat exchanger. Turbulence plays a crucial role in convective heat transfer, facilitating better fluid mixing and enhancing thermal exchange between the fluid and the heat transfer surfaces.

Furthermore, the direct proportionality of the enhancement to the number of baffles and Reynolds number underscores the significance of these parameters in influencing heat transfer performance. Increasing the number of baffles enhances the disruption and mixing of the fluid flow, fostering greater heat transfer. The Reynolds number, indicative of the flow regime, also plays a pivotal role, as the observed enhancements are particularly significant within the specified range.

The friction factor, indicative of pressure drop, exhibited consistently higher values in configurations with baffles compared to the no-baffle case as depicted in Fig. 12. This heightened friction is attributed to the creation of local stagnation points by baffles, augmenting momentum and subsequently increasing friction in the flow.

The friction factor of the wedge-bPHE is notably increased by 41% to 63%, whereas the aerofoil-bPHE shows an enhancement of 35% to 43% compared to conventional FPHE. However, the friction factor of the aerofoil-bPHE is considerably lower than that of the wedge-bPHE. These

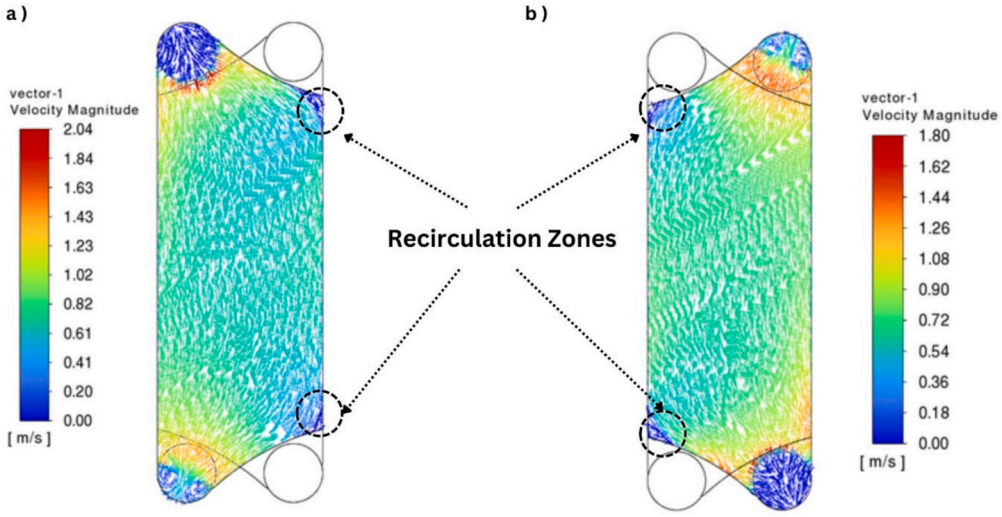


**Fig. 7.** (a & b) Recirculation zones in the conventional FPHE for hot and cold sides.

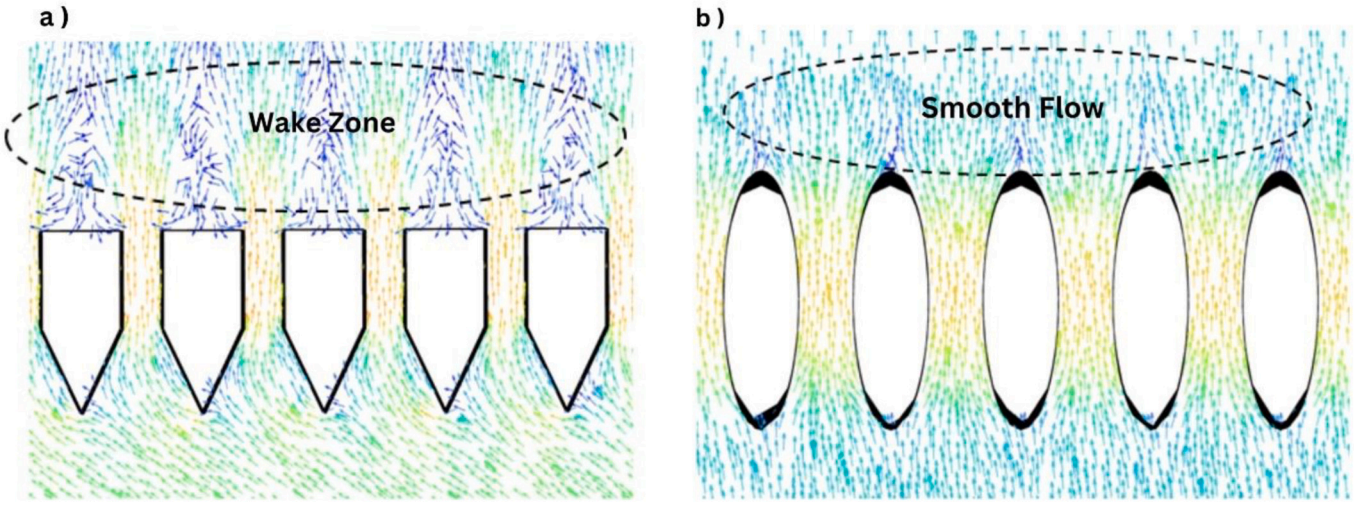


**Fig. 8.** (a) Wake and recirculated flow behind the wedge-bPHE (b) Smooth flow behind the aerofoil-bPHE.

streamlined baffles proved effective in reducing stagnation and wake zones, thereby mitigating pressure drop and friction factor.

Up to *Re* 500, friction factor values for all seven configurations were nearly identical, after which wedge-type baffles demonstrated higher friction factor values. At a Re of 500, there is an absence of discernible differences between the modified bPHE and the conventional counterpart. Subsequently, as the *Re* surpasses this threshold, the friction factor begins to rise. Following the transition from laminar to turbulent flow regimes, the modified bPHE exhibits a notable improvement in the friction factor, resulting in a higher pressure drop, particularly in the case of the wedge-bPHE with 3 and 5 baffles while all other cases show minimal alterations in the friction factor. This underscores the substantial impact of the Reynolds number and baffle configuration on the frictional characteristics of the modified bPHE.

Reynolds number, representing the ratio of inertial force to viscous force, and Stanton number, representing the ratio of heat transfer to thermal capacity, exhibited a consistent decrease in Stanton number with increasing Reynolds number for all configurations, including the no-baffle case. This reduction of Stanton number as a function of Reynolds number states that the inertia emphasized in the flow is higher than the contribution of heat transfer. This is illustrated in Fig. 13, where it is evident that the *St* value for bPHE is significantly greater, reaching up to 1.9, as opposed to the conventional counterpart, which only reaches 1.

The wedge baffle with five baffles yielded a higher Stanton number, indicating increased heat transfer in this configuration. This is attributed to the disruptive effect of wedge structures on flow, intensifying turbulence and heat transfer. In contrast, aerofoil baffles demonstrated comparatively lower heat transfer characteristics. In this observation, it is also noted that the scenario with a single wedge baffle and the one with five aerofoil baffles closely align and exhibit nearly identical St values. Furthermore, in the case of aerofoil baffles, the number of baffles has minimal influence on *St*, whereas a significant impact is observed in the case of wedge baffles.

Among all the configurations, the wedge type with five baffles exhibited the maximum friction factor, while the aerofoil with one baffle displayed the lowest value. To quantify these variations, a ratio of friction factors ($f_b$) for the six baffle configurations was linearized as a function of the friction factor value of the no-baffle case ($f_c$), serving as an effective relative friction factor and is interpreted in Fig. 14.

The least deviation in this factor (1.4) was observed in the case of aerofoil with one baffle, while the maximum deviation (1.6) occurred in the wedge type with five baffles. The data reveals a notable increase in this factor for the 3 and 5-wedge baffle cases. Conversely, the one wedge

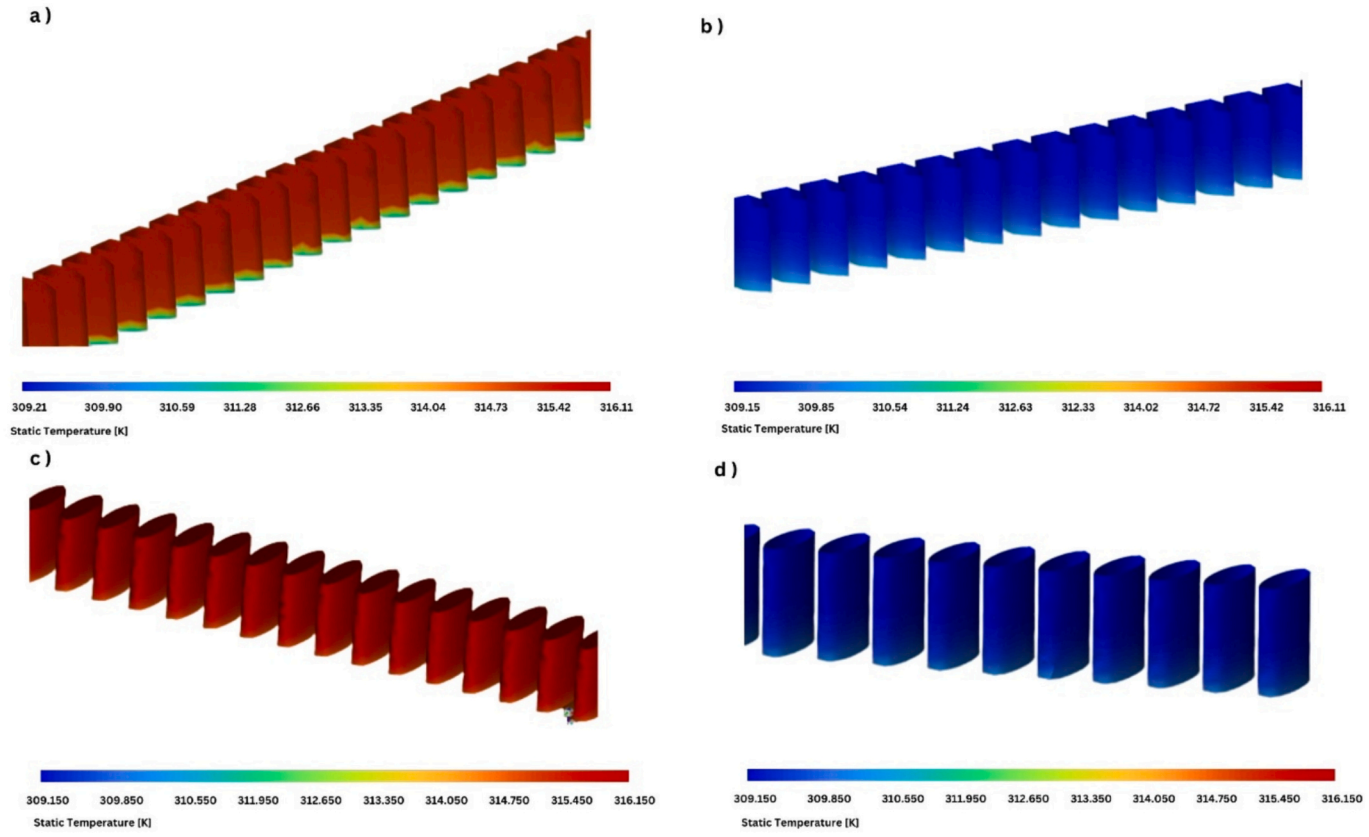


**Fig. 9.** Thermal diffusion through (a & b) wedge and (c & d) aerofoil baffle faces of hot and cold sides respectively.

baffle and the aerofoil configuration with three baffles exhibit nearly identical relative friction factors.

The interpretation of the relative *St* ratio in Fig. 15. indicates a significant rise, particularly for the wedge with 5 baffles, reaching up to 1.52. The wedge with 3 baffles also demonstrates an enhanced value of 1.47. In contrast, all other baffle cases exhibit much lower ratios, all falling below 1.42. This suggests that the configurations with five and three wedge baffles have a more pronounced impact on the *St* ratio compared to other cases, signifying a notable increase in the heat transfer performance.

Fig. 16. represents a notable outcome of this study which provides a valuable ratio for evaluating the thermal performance of PHEs. This ratio provides a clear indication of the comparative measure of heat transfer relative to pressure drop. The PEC reveals that wedge-type bPHEs outperform aerofoil types, with wedge-5 baffles demonstrating the best heat transfer efficiency. Despite the associated pressure drop costs, wedge-5 baffles exhibit superior performance with a PEC of 1.3, while wedge-3 baffles also provide commendable heat transfer performance with a PEC of 1.27. In contrast, aerofoil baffles exhibit significantly lower heat transfer efficiency. Additionally, it is noted that, except for wedge-3 and wedge-5 baffles, the performance of other cases declines as *Re* increases. However, the performance of wedge-5 baffles shows a positive correlation with *Re*.

As the Re increases, the performance of the aerofoil with 3 baffles initially decreases and eventually converges with that of the aerofoil with 1 baffle. This trend highlights a decline in performance as the flow rate or fluid velocity increases. Ultimately, the convergence with the aerofoil with 1 baffle suggests that the overall performance of the aerofoil-type plate heat exchanger is not optimal under higher Reynolds numbers, and the addition of baffles does not significantly enhance its heat transfer efficiency in comparison to configurations with fewer baffles.

The performance of the aerofoil with 5 baffles is notably inferior to that of the wedge with one baffle. However, there is a slight improvement in performance as the $Re > 1000$. This observation underscores the inherent disadvantage of the aerofoil model, even when equipped with 5 baffles, as it fails to compete effectively with the heat transfer efficiency exhibited by the wedge-type configuration. Despite a modest enhancement at higher Reynolds numbers, the overall performance of the aerofoil with 5 baffles remains suboptimal compared to the more favorable characteristics of the wedge-type PHE with a single baffle.

Overall, these findings underscore the effectiveness of wedge-type configurations, particularly wedge-5 baffles, in achieving a favorable balance between heat transfer performance and pressure drop costs.

**Advantages of baffled PHEs:**

The incorporation of baffles in PHEs is pivotal for enhancing heat transfer efficiency, especially in scenarios with marginal temperature differentials between fluids. Baffles offer multiple advantages, including the promotion of turbulence in fluid flow, extending residence time for more effective heat exchange, acting as conduits for heat conduction, and ensuring improved thermal stratification with a uniform temperature distribution. These features collectively make baffles essential components, optimizing heat exchange performance across diverse operating conditions and facilitating efficient thermal energy transfer in PHE systems.

## 5. Conclusions

In conclusion, the introduction of baffles in PHEs significantly influences flow characteristics, pressure drop, and heat transfer. The choice between wedge-type and aerofoil-type baffles has notable implications for the performance of the heat exchanger.

Wedge-type baffles, characterized by a bluff body, create flow detachment at the rear, resulting in a visible wake zone and increased turbulence. This configuration leads to higher pressure drop and turbulent intensity within the PHE. On the other hand, aerofoil-type baffles

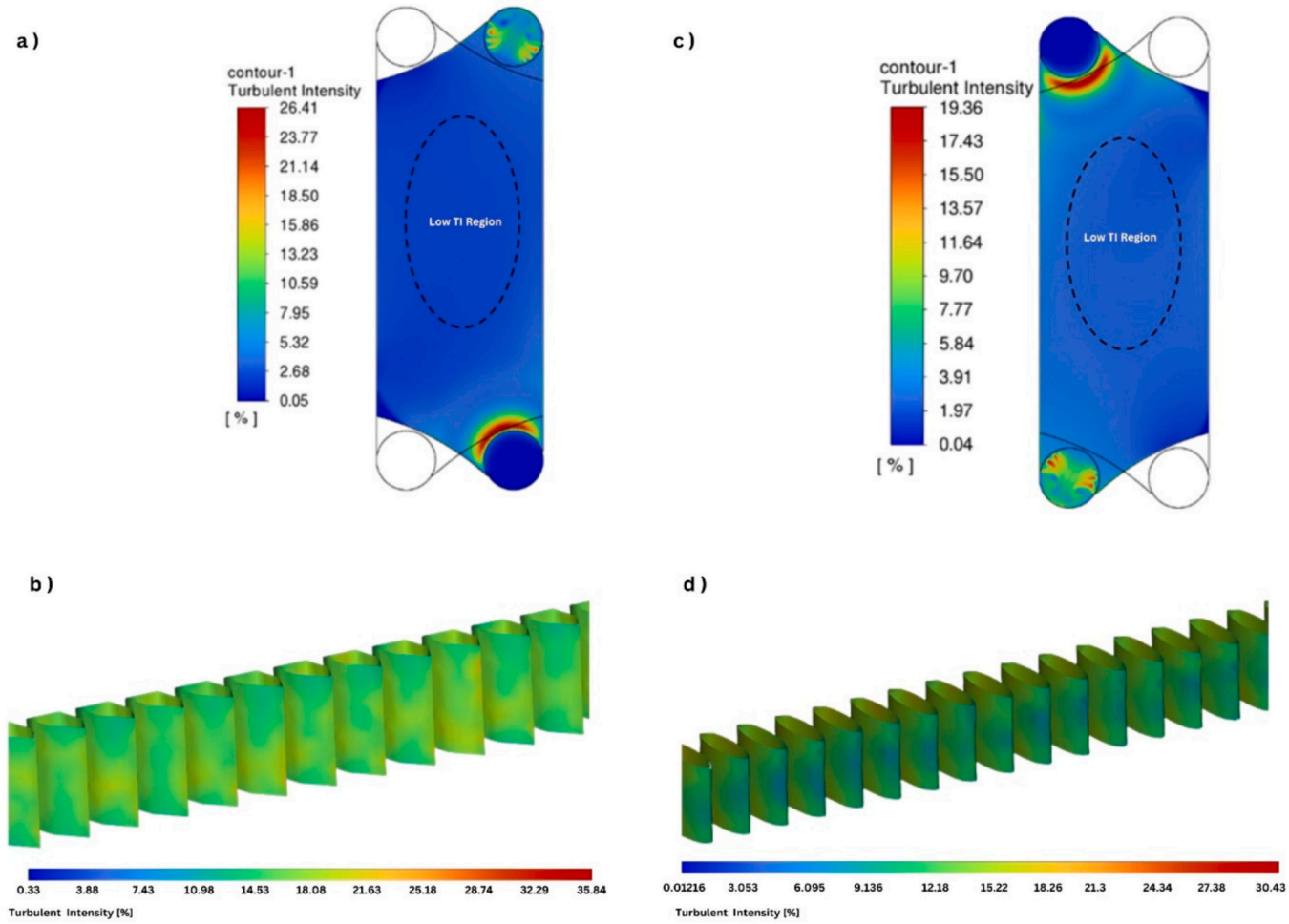


**Fig. 10.** (a & c) Lower turbulent region of conventional FPHE (b & d) Higher turbulent region across the wedge and aerofoil baffles respectively.

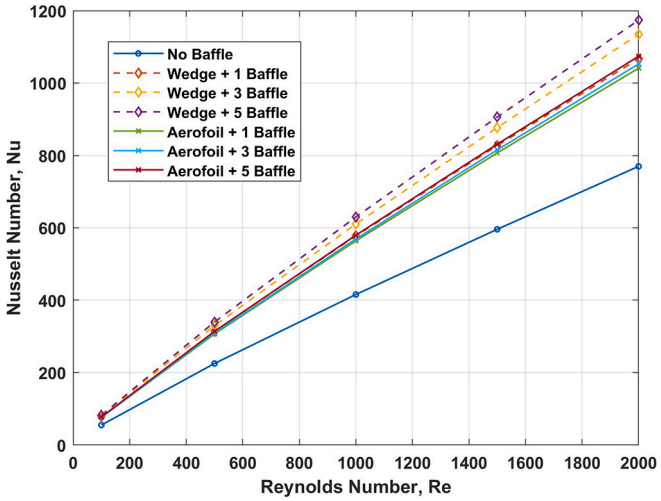


**Fig. 11.** Nusselt number for all the bPHE configurations and conventional FPHE.

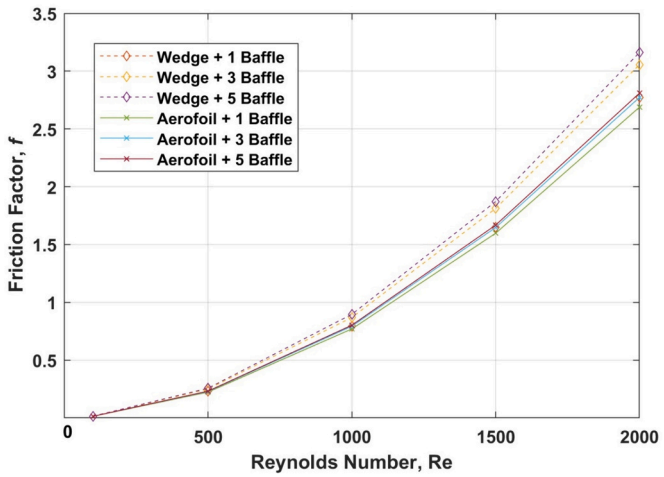


**Fig. 12.** Friction factor for all the bPHE configurations and conventional FPHE.

minimize stagnation at the front and exhibit a smaller wake zone, resulting in lower pressure drop and turbulent intensity. The baffles itself act as heat dissipation bodies, facilitating conduction and contributing to enhanced heat transfer.

- The Nusselt number analysis indicates a substantial increase in heat transfer for both 5-wedge-baffle and 5-aerofoil-baffle setups, with wedge-baffles showing a more significant enhancement. Specifically, for 5 wedge-baffle case, there is significant enhancement of upto 55%.
- The wedge-baffle configuration has higher TKE compared to aerofoil. And the heat transfer enhancement directly depends on the number

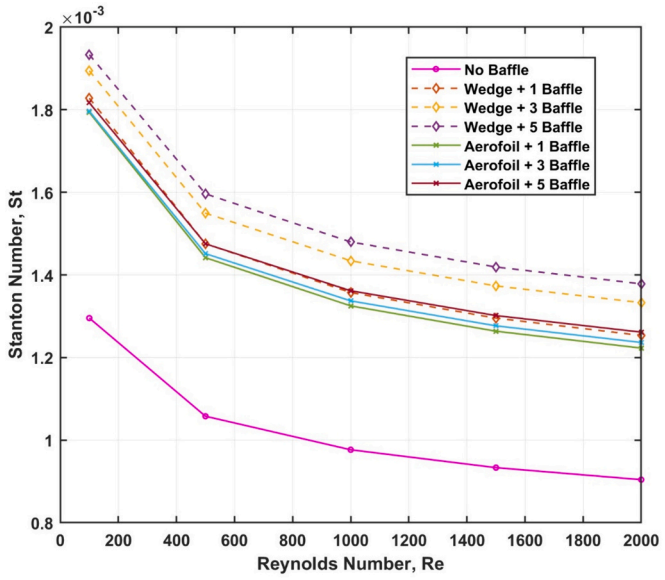


**Fig. 13.** Stanton number for all the bPHE configurations and conventional FPHE.

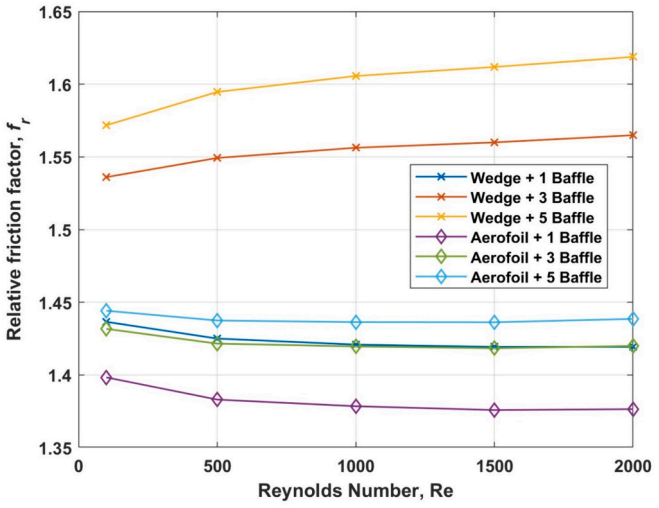


**Fig. 14.** Relative *f* factor for all the bPHE configurations and conventional FPHE.

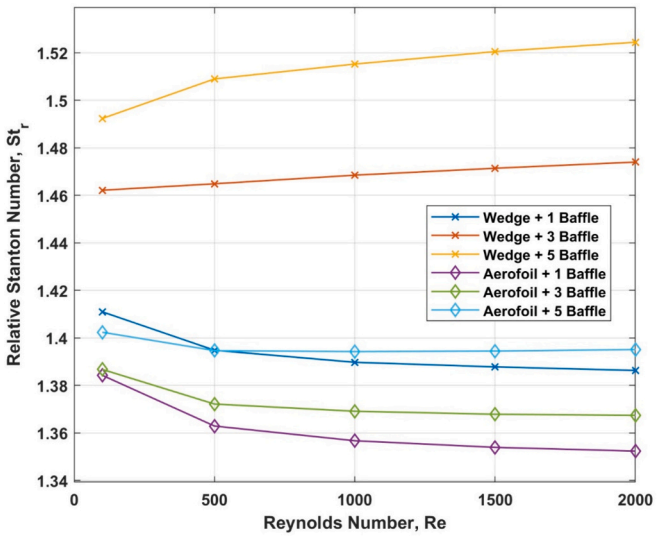


**Fig. 15.** Relative *St* factor for all the bPHE configurations and conventional FPHE.

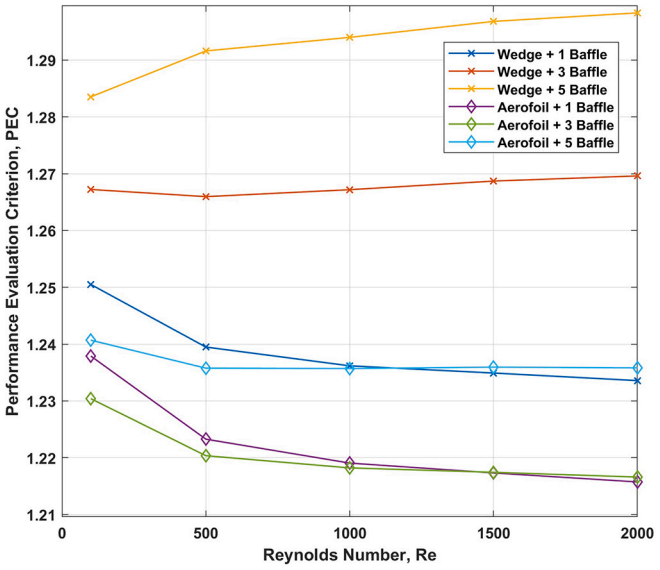


**Fig. 16.** PEC for all the bPHE configurations.

of baffles. Specifically, the number of baffles have higher impact for wedge bPHE. For instance, for *Re* 2000, the 3 wedge-configuration has 10% higher both *Nu* and *St* as compared to that 1 wedge whereas for aerofoil, 3 baffles has 3% enhancement to that 1 baffle. It is observed that as *Re* increases, the *Nu* is decreased for all 5 configurations except wedge-bPHE with 3 and 5 baffles.

- The aerofoil bPHE has lower pressure drop as compared to wedge bPHE upto 12%. The friction factor of the wedge-bPHE is notably increased by 41% to 63%, whereas the aerofoil-bPHE shows an enhancement of 35% to 43% compared to conventional FPHE. Up to *Re* 500, friction factor enhancement for all seven configurations were nearly identical. It is observed that as *Re* increases, the *f* is decreased for all 5 configurations except wedge-bPHE with 3 and 5 baffles.
- *St* value for bPHE is significantly greater, reaching up to 1.9, as compared to the conventional one of *St* value 1. The wedge-configuration with the number of baffles three (46% to 48%) and five (49% to 53%) showed higher enhancement of *St* while all aerofoil-configurations (40% to 35%) and wedge-configuration with one baffle (41% to 39%) has relatively lower *St*.
- The performance of the aerofoil with 5 baffles is notably inferior to that of the wedge with one baffle though there is a slight improvement in performance as the $Re > 1000$.
- The least deviation in the relative friction factor $f_r$ (1.3) was observed in the case of aerofoil with one baffle, while the maximum deviation (1.6) occurred in the wedge type with five baffles.
- The relative Stanton number $St_r$ for wedge with 5 and 3 baffles, demonstrates an enhanced value of 1.52 and 1.47 respectively. In contrast, all other baffle cases exhibit much lower ratios, all falling below 1.42.
- The PEC of wedge and aerofoil type is about 1.24 to 1.3 and 1.21 to 1.24 to that of conventional one respectively. The wedge-5 and 3 baffles exhibit superior performance with a PEC of 1.3 and 1.27 respectively.

Considering both hydrodynamic and thermodynamic aspects, the wedge-bPHE performs optimal compared to that of the aerofoil-bPHE.

They exhibit optimal balance between the heat transfer coefficient and pressure drop. For optimized heat exchanger performance, the configuration featuring wedge-bPHE with five baffles appears to be a promising choice.

In case of necessity of lower pressure drop with some compromising heat transfer rate, the aerofoil-bPHE with five baffles and wedge-bPHE with one baffle (PEC of 1.24 both) are preferrable.

**Future Research and Outlook:**

The lack of comprehensive literature on the integration of baffles in PHEs highlights a critical area for future research. Detailed studies are necessary to explore various baffle designs, placement strategies, and their impact on heat transfer performance and operational efficiency in PHEs. Additionally, investigations into different applications and operating conditions will provide valuable insights for optimizing baffle integration and reaping maximum benefits in diverse industrial settings.

In conclusion, incorporating baffles in PHEs presents a promising avenue for enhancing heat transfer efficiency, although further research and experimentation are warranted to fully understand the extent of the benefits and the optimal design parameters.

## CRediT authorship contribution statement

**M. Nithya:** Writing – original draft, Validation, Software, Project administration, Methodology, Investigation, Conceptualization. **M. Senthil Vel:** Investigation, Visualization, Resources, Software. **S. Anitha:** Writing – review & editing. **C. Sivaraj:** Writing – review & editing, Supervision.

## Declaration of competing interest

The authors declare that they have no known competing financial interests or personal relationships that could have appeared to influence the work reported in this paper.

## Data availability

Data will be made available on request.

## Acknowledgments

We express our sincere gratitude to Mr. M. Muruganantham, Additional Chief Manager, and Mr. S. Ganapathi, Chief Manager, at NTPL, Tuticorin, for their unwavering support in various facets, such as technical assistance, supplying necessary data, and sharing profound expertise in the relevant field. We would like to express our gratitude to PSG College of Arts and Science for generously providing a stipend to support our research endeavours. Additionally, we extend our heartfelt appreciation to PSG Institute of Technology and Applied Research, Coimbatore for backing our project by offering a dedicated workstation.

## References

[1] D.J.B. Clark, Plate Heat Exchanger Design and Development, 1976.
[2] Gasketed Plate Heat Exchanger Market Size, Share, Competitive Landscape and Trend Analysis Report by Type, by Material, by End User : Global Opportunity Analysis and Industry Forecast, 2021–2031, Allied Market Research, 2022.
[3] P. Kapustenko, J.J. Klemeš, O. Arsenyeva, Plate heat exchangers fouling mitigation effects in heating of water solutions: a review, Renew. Sust. Energ. Rev. 179 (2023) 113283.
[4] K.S. Mushatet, A review study for a twisted tube heatexchange, J. Nanofluids (2023) 299–317.
[5] A. Boonloi, W. Jedsadaratanachai, 3D-numerical predictions of flow structure and heat transfer behavior in heat exchanger tubes inserted with different patterns of double-V baffles, Case Stud. Therm. Eng. 39 (2022) 102385.
[6] A.S. Soliman, et al., Numerical investigation of the Ribs' shape, spacing, and height on heat transfer performance of turbulent flow in a flat plate heat exchanger, Sustainability 14 (22) (2022) 15143.
[7] F. Montazerifar, M. Amidpour, Z. Abedi, Numerical investigation of turbulent nanofluid flow behavior in a multi-stream plate-fin heat exchanger with a novel design of fractal fins, Alexand. Eng. J. 72 (2023) 431–449.
[8] X. Lianzheng, et al., Operation characteristics of air–air heat pipe inserted plate heat exchanger for heat recovery, Energy Build. 185 (2019) 66–75.
[9] S. Marzouk, et al., Thermo-hydraulic study in a shell and tube heat exchanger using rod inserts consisting of wire-nails with air injection: experimental study, Int. J. Therm. Sci. 161 (2021) 106742.
[10] Z. Feng, et al., Combined influence of rectangular wire coil and twisted tape on flow and heat transfer characteristics in square mini-channels, Int. J. Heat Mass Transfer 205 (2023) 123866.
[11] M.B. Sarasar, et al., The effect of vortex generator insert and $TiO_2$/Water nanofluid on thermal efficiency and heat transfer of flat plate solar collector, Sustain. Energy Technol. Assess. 53 (2022) 102617.
[12] K. Deepika, R. Sarviya, Application based review on enhancement of heat transfer in heat exchangers tubes using inserts, Mater. Today: Proceed. 44 (2021) 2362–2365.
[13] N.K. Panday, S.N. Singh, Study of thermo-hydraulic performance of chevron type plate heat exchanger with wire inserts in the channel, Int. J. Therm. Sci. 173 (2022) 107360.
[14] I. Gherasim, et al., Heat transfer and fluid flow in a plate heat exchanger part I. Experimental investigation, Int. J. Therm. Sci. 50 (8) (2011) 1492–1498.
[15] M. Piper, et al., Heat transfer enhancement in pillow-plate heat exchangers with dimpled surfaces: a numerical study, Appl. Therm. Eng. 153 (2019) 142–146.
[16] F. Tetsu, et al., Influence of various surface roughness on the natural convection, Int. J. Heat Mass Transfer 16 (3) (1973) 629–636.
[17] H. Kang, T. Wong, C.W. Leung, Effect of surface roughness on cost effectiveness of equilateral triangular passage heat exchanger, HKIE Transact. 6 (2) (1999) 26–31.
[18] S. Seok, et al., A study on the effects of etching surface characteristics on condensation heat transfer in pre-heating exchanger, J. Energy 23 (2) (2014) 217–222.
[19] J. Wajs, D. Mikielewicz, Effect of Surface Finish on Heat Transfer Performance of Plate Heat Exchanger, HEFAT (2012).
[20] M. Attalla, H.M. Maghrabie, An experimental study on heat transfer and fluid flow of rough plate heat exchanger using $Al_2O_3$/water nanofluid, Exper. Heat Trans. 33 (3) (2020) 261–281.
[21] J. Wajs, D. Mikielewicz, Effect of surface roughness on thermal-hydraulic characteristics of plate heat exchanger, Key Eng. Mater. 597 (2014) 63–74.
[22] T. Ohara, et al., Heat transfer and pressure drop of boiling flow in a cross-ribbed flat channel, Int. Commun. Heat Mass Transfer 17 (5) (1990) 555–566.
[23] G. Tanda, et al., Natural convection heat transfer from a ribbed vertical plate: effect of rib size, pitch, and truncation, Exper. Therm. Fluid Sci. 145 (2023) 110898.
[24] J. Hærvig, H. Sørensen, Natural convective flow and heat transfer on unconfined isothermal zigzag-shaped ribbed vertical surfaces, Int. Commun. Heat Mass Transf. 119 (2020) 104982.
[25] B. Nghana, F. Tariku, G. Bitsuamlak, Numerical study of the impact of transverse ribs on the energy potential of air-based BIPV/T envelope systems, Energies 16 (14) (2023) 5266.
[26] K. Nilpueng, S.J.E.T. Wongwises, F. Science, Experimental study of single-phase heat transfer and pressure drop inside a plate heat exchanger with a rough surface, Exper. Therm. Fluid Sci. 68 (2015) 268–275.
[27] C. Gulenoglu, et al., Experimental comparison of performances of three different plates for gasketed plate heat exchangers, Int. J. Therm. Sci. 75 (2014) 249–256.
[28] S. Al-zahrani, M.S Islam, S.C. Saha, Heat transfer enhancement investigation in a novel flat plate heat exchanger, Int. J. Therm. Sci. 161 (2021) 106763.
[29] S. Al-zahrani, M.S. Islam, S.C. Saha, Heat transfer enhancement of modified flat plate heat exchanger, Appl. Therm. Eng. 186 (2021) 116533.
[30] S. Al-zahrani, M.S. Islam, S.C. Saha, Heat transfer augmentation in retrofitted corrugated plate heat exchanger, Int. J. Heat Mass Transfer 161 (2020) 120226.
[31] S. Al-zahrani, M.S. Islam, S.C. Saha, Heat transfer enhancement of modified flat plate heat exchanger, Appl. Therm. Eng. 186 (2021) 116533.
[32] P. Bichkar, et al., Study of shell and tube heat exchanger with the effect of types of baffles, Procedia Manuf. 20 (2018) 195–200.
[33] J. Chen, et al., Experimental thermal-hydraulic performances of heat exchangers with different baffle patterns, Energy 205 (2020) 118066.
[34] X. Xiao, et al., Numerical investigation of helical baffles heat exchanger with different Prandtl number fluids, Int. J. Heat Mass Transf. 63 (2013) 434–444.
[35] B.A. Abdelkader, S.M. Zubair, The effect of a number of baffles on the performance of shell-and-tube heat exchangers, Heat Transf. Eng. 40 (1–2) (2019) 39–52.
[36] A. El Maakoul, et al., Numerical design and investigation of heat transfer enhancement and performance for an annulus with continuous helical baffles in a double-pipe heat exchanger, Energy Convers. Manag. 133 (2017) 76–86.
[37] L. He, P. Li, Numerical investigation on double tube-pass shell-and-tube heat exchangers with different baffle configurations, Appl. Therm. Eng. 143 (2018) 561–569.
[38] S.J. Kline, The Purposes of Uncertainty Analysis, ASME J. Fluids Eng. (1985).
[39] Ansys, Ansys Fluent 12.0 User's Guide, 2009.
[40] J.L. Lumley, Turbulence modeling 50 (1983) 1097–1103.
[41] J. John, et al., Computational fluid dynamics simulation of the turbulence models in the tested section on wind tunnel, Ain Shams Eng. J. 11 (4) (2020) 1201–1209.
[42] Y. Wu, et al., Three-dimensional simulation for an entrained flow coal slurry gasifier, Energy Fuels 24 (2) (2010) 1156–1163.
[43] R. Kumar, et al., CFD based analysis heat transfer and friction characteristics of broken multiple rib roughened solar air heater duct, Int. J. Mech. Prod. Eng. Res. Develop. 172 (2013).
[44] M. Pourramezan, H. Ajam, Modeling for thermal augmentation of turbulent flow in a circular tube fitted with twisted conical strip inserts, Appl. Therm. Eng. 105 (2016) 509–518.

[45] R. Zhang, et al., Effects of turbulence models on forced convection subcooled boiling in vertical pipe, Annals Nucl. Energy 80 (2015) 293–302.
[46] S. Khajehhasani, B.A. Jubran, Comparison of various turbulence models to predict film cooling effectiveness from different exit shaped holes with sister holes influence, in: Proc. 21st Annual Conference of the CFD Society of Canada, 2013.
[47] Z. Quan, et al., Pressure drop in seven-pin wire-wrapped rod bundle for the sodium cartridge loop in versatile test reactor, Nucl. Sci. Eng. 197 (5) (2023) 771–787.
[48] M.S. Cellek, Turbulent flames investigation of methane and syngas fuels with the perspective of near-wall treatment models, Int. J. Hydrogen Energy 45 (60) (2020) 35223–35234.
[49] S. Alimirzazadeh, et al., GPU-accelerated Pelton turbine simulation using finite volume particle method coupled with linear eddy viscosity models, in: IOP Conference Series: Earth and Environmental Science, IOP Publishing, 2019.